Since January 2020 Elsevier has created a COVID-19 resource centre with free information in English and Mandarin on the novel coronavirus COVID-19. The COVID-19 resource centre is hosted on Elsevier Connect, the company's public news and information website.

Virology 567 (2022) 1–14

Contents lists available at ScienceDirect

Virology

journal homepage: www.elsevier.com/locate/virology

Analysis of a crucial interaction between the coronavirus nucleocapsid protein and the major membrane-bound subunit of the viral replicase-transcriptase complex

Cheri A. Koetzner [a], Kelley R. Hurst-Hess [a], Lili Kuo [a], Paul S. Masters [a,b,*]

[a] Laboratory of Viral Replication and Vector Biology, Wadsworth Center, New York State Department of Health, Slingerlands, NY, 12159, USA
[b] Department of Biomedical Sciences, School of Public Health, State University of New York, Albany, NY, 12208, USA

ARTICLE INFO

Keywords:
Coronavirus
Viral genomic RNA
Viral RNA synthesis
Mouse hepatitis virus
Nucleocapsid protein
Nonstructural protein 3

ABSTRACT

The coronavirus nucleocapsid (N) protein comprises two RNA-binding domains connected by a central spacer, which contains a serine- and arginine-rich (SR) region. The SR region engages the largest subunit of the viral replicase-transcriptase, nonstructural protein 3 (nsp3), in an interaction that is essential for efficient initiation of infection by genomic RNA. We carried out an extensive genetic analysis of the SR region of the N protein of mouse hepatitis virus in order to more precisely define its role in RNA synthesis. We further examined the N-nsp3 interaction through construction of nsp3 mutants and by creation of an interspecies N protein chimera. Our results indicate a role for the central spacer as an interaction hub of the N molecule that is partially regulated by phosphorylation. These findings are discussed in relation to the recent discovery that nsp3 forms a molecular pore in the double-membrane vesicles that sequester the coronavirus replicase-transcriptase.

1. Introduction

The nucleocapsid (N) protein is a major structural component of the coronavirus virion. N wraps the RNA genome into a ribonucleoprotein complex that is assembled into virions via contacts with the viral membrane (M) protein, the carboxy terminus of which projects into the interior of the enveloped viral particle. N-RNA, N–N, and N-M interactions are crucial to virus assembly, and some of these are fairly well characterized (de Haan and Rottier, 2005; Hogue and Machamer, 2008). N proteins spanning all of the four genera of the coronavirus family exhibit a highly conserved architecture (Fig. 1A), despite having more limited amino acid sequence homology across the same phylogenetic distance. The N molecule contains two independent structural domains, designated NTD and CTD, each of which binds to RNA (Chang et al., 2014). Additionally, the CTD interlocks N monomers into dimers. The N3 domain, at the extreme carboxy terminus of the molecule, is responsible for interaction with the carboxy terminus of the M protein (Hurst et al., 2005; Verma et al., 2006; Kuo et al., 2016). N3 also mediates tetramerization of N dimers (Ye et al., 2020). Both the NTD and the CTD are flanked by polypeptide linkers that are thought to be unstructured or intrinsically disordered. The largest of these, the N2a spacer between the NTD and the CTD, encompasses a serine- and arginine-rich (SR) region at its upstream end.

Less clearly defined is the function of N protein in coronavirus RNA synthesis, an intricate process that entails both replication of full-length (~30 kb) genomic RNA (gRNA), as well as transcription of a 3′-nested set of smaller subgenomic (sg) mRNA species (Sola et al., 2015). Coronavirus RNA synthesis is carried out by the viral replicase-transcriptase complex (RTC), an assemblage comprising 16 nonstructural protein (nsp) constituents, which are encoded as a polyprotein by the 5′-most two-thirds of the genome. This machinery is sequestered by double-membrane vesicles that are generated by the action of a subset of the nsps during the onset of infection (Snijder et al., 2020). It has consistently been observed that a fraction of N protein colocalizes with some RTC components at an early stage as well as later in infection, suggesting that N participates in RNA synthesis (van der Meer et al., 1999; Sims et al., 2000; Stertz et al., 2007; Ulasli et al., 2010). Moreover, studies carried out with replicons of various coronaviruses have shown that, although it is not absolutely required, N protein greatly stimulates RNA synthesis. However, these studies did not establish the mechanistic basis for this dependence, and evidence was conflicting as to whether the effect of N is principally exerted at the level of gRNA replication

* Corresponding author. Laboratory of Viral Replication and Vector Biology, Wadsworth Center, New York State Department of Health, Slingerlands, NY, 12259, USA.
E-mail address: Paul.Masters@health.ny.gov (P.S. Masters).

https://doi.org/10.1016/j.virol.2021.12.004
Received 9 September 2021; Received in revised form 10 December 2021; Accepted 12 December 2021
Available online 14 December 2021

(Thiel et al., 2001; Schelle et al., 2005) or sgRNA transcription (Almazán et al., 2004; Zúñiga et al., 2010). A singular manifestation of the functional importance of N protein is that, distinct from almost all other positive-strand RNA virus genomes, purified or synthesized coronavirus gRNA is only minimally infectious when transfected into host cells. By contrast, N protein, usually supplied as cotransfecting N mRNA, dramatically enhances the infectivity of gRNA (Casais et al., 2001; Coley et al., 2005; Yount et al., 2000, 2002, and 2003).

A clue to the role of N protein in RNA synthesis came from our discovery of a previously unsuspected interaction between N and nsp3, the largest of the RTC subunits. This finding originated with a genetic analysis of the N protein of the prototype coronavirus mouse hepatitis virus (MHV) and that of its close relative, bovine coronavirus (BCoV) (Hurst et al., 2010). Although the respective N proteins of MHV and BCoV are highly homologous, substitution of the BCoV N protein in place of its counterpart in the MHV genome resulted in a mutant that was only minimally viable. Reverting mutations that repaired the severely defective substitution mutant mapped to two sites. The first of these was the SR region of the N protein, which is the most divergent segment between the BCoV and MHV N proteins. The second locus of reverting mutations was in nsp3, specifically the amino-terminal ubiquitin-like (Ubl1) domain plus part of the adjacent acidic region (Ac), a portion of the molecule sometimes denoted as nsp3a or nsp3^{N}. Similarly, an incompatible substitution in MHV of the SR region of the N protein of severe acute respiratory syndrome coronavirus (SARS-CoV) evoked the selection of reverting mutations in both the N SR region and nsp3. Biochemical support for the interaction between N and nsp3 was obtained from assays in which Ubl1-Ac fused to glutathione S-transferase (GST) was shown to pull down N protein from lysates of MHV-infected cells. Further physical confirmation of the N-nsp3 interaction was presented in a study by Keane and Giedroc, in which high-affinity binding between these two components was measured by isothermal calorimetry (Keane and Giedroc, 2013). This work found that the N protein SR region is the major determinant of binding to Ubl1, but there is also a significant contribution made by the NTD.

Notably, the N-nsp3 interaction was found to coincide with the

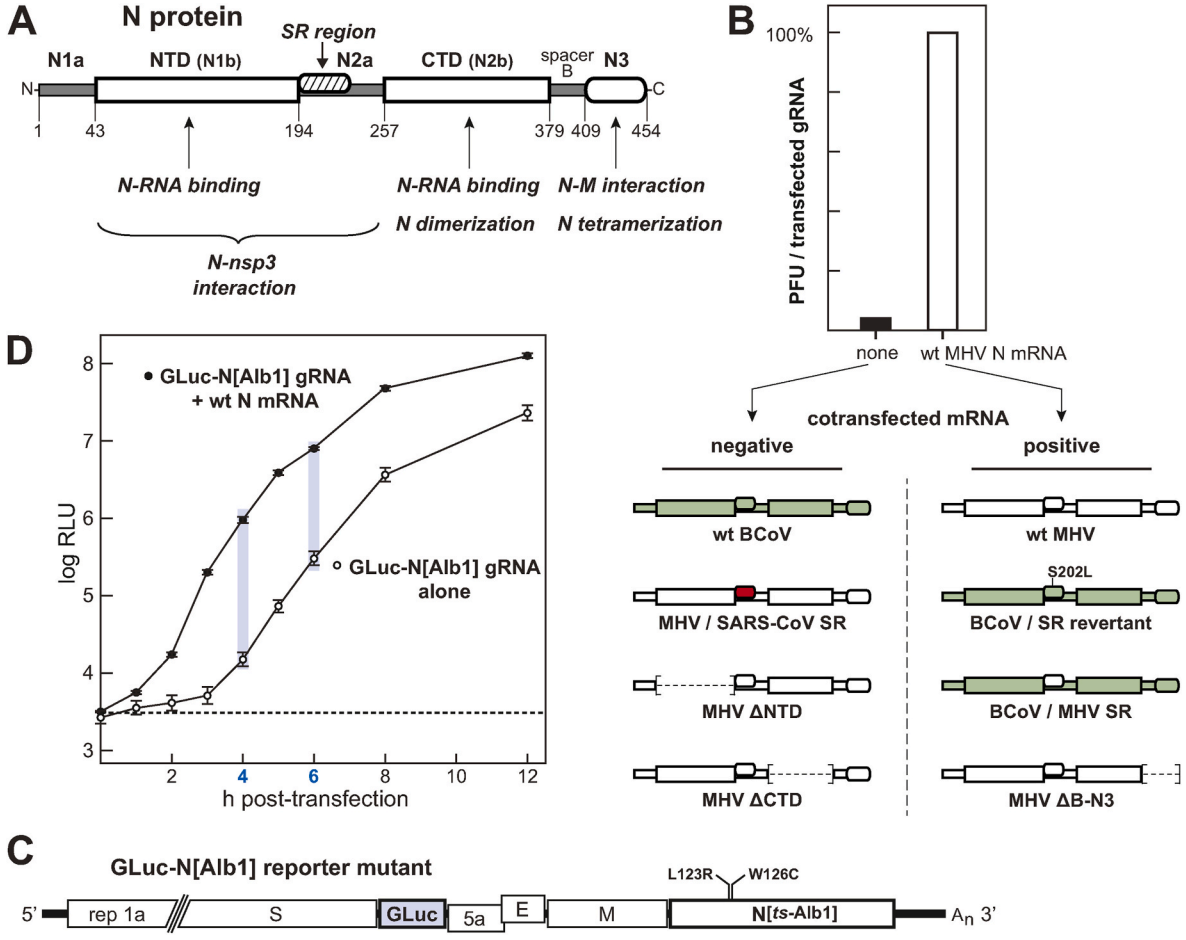

Fig. 1. N protein structure and stimulation of gRNA infectivity by N protein. (A) Domain structure of the coronavirus N protein. Two highly structured domains, designated NTD and CTD (alternately called N1b and N2b, respectively), each have RNA-binding activity (Chang et al., 2014); the CTD also tightly dimerizes N monomers. The carboxy-terminal N3 domain mediates assembly of the nucleocapsid into virions through interaction with the carboxy-terminal tail of the M protein (Hurst et al., 2005; Verma et al., 2006; Kuo et al., 2016); N3 also brings together N dimers to form tetramers (Ye et al., 2020). Unstructured spacer segments (N1a, N2a and spacer B) flank the NTD and CTD; the N2a spacer contains the serine- and arginine-rich (SR) region at its upstream end. Amino-acid residue numbers shown below the schematic are those for the MHV N protein. (B) Summary of some previous results for stimulation of MHV gRNA infectivity by cotransfected N mRNA. (C) Genomic elements of the GLuc-N[Alb1] reporter mutant constructed for cotransfection assays. The GLuc gene from *Gaussia princeps* (blue), inserted in place of the nonessential accessory gene 4, encodes a secreted luciferase. The N gene of MHV mutant Alb1 contains two closely spaced mutations in the NTD that render the N protein highly defective at the nonpermissive temperature (39 °C). The portion of the genome between the 5′ end and the S gene, which is identical to that of wild-type MHV, is not shown. (D) Kinetics of secreted luciferase signal development in mouse L2 cells at 39 °C, following transfection of GLuc-N[Alb1] gRNA (0.25 μg) with or without cotransfection of wild-type N mRNA (0.50 μg). Each point represents the mean of the logarithm of relative light units (RLU) (+/− standard deviation) from three separate transfections. Vertical bars (blue) indicate 4 h and 6 h post-transfection time points chosen for subsequent assays. Broken line, background autofluorescence of media from uninfected cells.

ability of N protein to upregulate the infectivity of gRNA, examples of which are summarized in Fig. 1B (Hurst et al., 2010, 2013). Accordingly, MHV gRNA infectivity could not be stimulated by the wild-type BCoV N protein or by a mutant MHV N protein containing the SARS-CoV SR region. Conversely, activity was restored in BCoV N protein containing either a reverting mutation or the entire MHV N SR region. In addition to the necessity of matching the SR region of N to a cognate Ubl1 domain of nsp3, stimulation of gRNA infectivity by N was found to also require intact RNA-binding ability. Thus, deletion of either the NTD or the CTD abrogated the enhancement of gRNA infectivity; similarly, specific individual NTD point mutants (R125A, Y127A, or Y190A) that lost the ability to bind RNA also were unable to support gRNA infectivity (Grossoehme et al., 2009; Keane et al., 2012). In contrast, removal of the M-interacting carboxy-terminal domain N3 had no effect on this activity (Fig. 1B). Taken together, these results strongly suggested that the underlying reason for the N protein requirement in coronavirus RNA synthesis is the necessity for N to interact with nsp3, potentially to ensure the productive engagement of the nascent RTC with its gRNA substrate.

This relationship has now been much more solidly established by multiple important findings from a recent study by the Reggiori and de Haan laboratories (Cong et al., 2020). First, these investigators performed a comprehensive yeast two-hybrid (Y2H) analysis with N protein and each of the 16 components (nsp1-nsp16) of the MHV RTC. This revealed that nsp3, and in particular the amino-terminal nsp3^{N}, is the only part of the RNA-synthetic machinery to interact with N protein. Second, using Y2H and GST pulldown, they found that N-nsp3 binding is mediated, possibly redundantly, by separate interactions mapping to both the NTD and spacer 2a (which contains the SR region). Finally, with expressed wild-type and mutant N proteins they demonstrated that recruitment of N to the RTC in infected cells is wholly dependent upon the N-nsp3 interaction.

In the work reported here, we undertook an extensive mutational analysis of the SR region of the MHV N protein in order to more precisely define its role in RNA synthesis. Additionally, we further probed the interaction between N and nsp3 through construction of Ubl1 point mutants and by generation of an interspecies N protein chimera. Our results point to the function of the N2a spacer, including the SR region, as an interaction hub of the N molecule that is regulated in part by phosphorylation.

2. Results

2.1. Optimization of an assay for gRNA - N mRNA cotransfection

To measure stimulation of gRNA infectivity by N mRNA we and others previously carried out plaque (or infectious centers) assays, which typically provide a readout at some 48–72 h post-transfection (Grossoehme et al., 2009; Hurst et al., 2010, 2013; Keane et al., 2012). In order to quantitatively examine events at much earlier times during infection we constructed an MHV mutant, GLuc-N[Alb1], which then served as the source of gRNA for cotransfection assays. This mutant contained two critical elements (Fig. 1C). First, to act as a reporter, the GLuc gene from *Gaussia princeps* was inserted in place of gene 4, the gene for a truncated nonessential accessory protein in MHV-A59 (de Haan et al., 2002). GLuc encodes a small (19 kDa) luciferase that is secreted into cell media and has a very high bioluminescent signal intensity (Tannous et al., 2005). Second, the wild-type N gene was replaced with that of the Alb1 virus, a mutant that is temperature-sensitive and thermolabile due to two mutations in its N protein NTD, L123R and W126C (Masters et al., 1994). We reasoned that, since the Alb1 N protein is minimally functional at 39 °C, this would reduce the contribution made to gRNA infectivity by the eventual transcription and translation of the N gene that is contained in the gRNA itself.

GLuc-N[Alb1] gRNA was electroporated into mouse L2 cells with or without cotransfected wild-type N mRNA, and aliquots of media were removed at various times post-transfection and assayed for luciferase activity (Fig. 1D). Cells were incubated at 39 °C because this is the nonpermissive temperature for Alb1; this also turned out to be the temperature at which we observed the most profound phenotypes of constructed N SR region mutants (see below). We found that, as expected, luciferase activity originating from transfected gRNA was greatly increased by the provision of cotransfected N mRNA. Nevertheless, the curve for the signal from gRNA alone was not flat. This may indicate that the requirement for N mRNA is not absolute. However, we believe a more likely explanation is that the Alb1 mutations render the N protein severely defective but still minimally functional, since the Alb1 mutant is still weakly viable at the nonpermissive temperature (Masters et al., 1994). The greatest rise in stimulation of luciferase activity by N mRNA was seen at 3–8 h post-transfection, during which gRNA infectivity was enhanced 30- to 100-fold, an increase of the same magnitude as previously observed in plaque assays. We chose to use time points of 4 h and 6 h post-transfection (Fig. 1D) for subsequent assays.

2.2. Effects of serine-to-alanine mutations in the SR region of N protein

The SR region constitutes the upstream half of the N2a segment linking the NTD and the CTD (Fig. 1A) and is a major locus of N protein phosphorylation (Peng et al., 2008; Wu et al., 2009; Davidson et al., 2020; Bouhaddou et al., 2020). In prior work we had found that single mutations of amino acid residues in this region did not detectably affect the stimulation of gRNA by N mRNA (data not shown). Accordingly, we examined the effects of changing groups of residues, focusing initially on converting serines to alanines, in order to abolish potential phosphorylation sites. One mutant of this set, S3A, altered the triplet of serines (S218–S220) near the downstream end of the SR region (Fig. 2A). A second mutant, S4A, was constructed to knock out four serines (S197, S201, S205, and S209) that are putative targets for glycogen synthase kinase-3 (GSK-3) (Wu et al., 2009). Another mutant, S7A, added three additional neighboring serine-to-alanine mutations to those in S4A. Finally, the S11A mutant altered all of the serines in the SR region.

When these mutations were incorporated into N mRNA used in cotransfection assays, we observed a gradient of attenuation in the ability to stimulate gRNA infectivity (Fig. 2B). The effect of the S3A mutations was minimal, suggesting that the downstream cluster of serines (S218–S220) are of relatively minor importance. By contrast, the functionality of N mRNA was severely diminished by the S4A mutations and still more so by the S7A mutations. No significant further reduction was seen with the S11A mutant N mRNA, consistent with the minor contribution of the S3A mutations. A similar trend was observed when the same serine-to-alanine mutations were incorporated into the N gene in the MHV genome, although there was not strict accord between the viral phenotype and the N mRNA phenotype. Plaques of the S3A mutant were indistinguishable from the wild type (not shown), while the S4A mutant formed plaques only slightly smaller than those of the wild type (Fig. 2C). On the other hand, the S7A and S11A mutations were lethal. These results showed that the serine residues at the upstream end of the SR region (S194–S209) are the ones most important for the interaction with nsp3 Ubl1 and possibly for other functions essential for viral viability.

2.3. Effects of serine-to-aspartate mutations in the SR region of N protein

We next constructed two mutants in which groups of serine residues were changed to aspartates, to mimic the effect of permanent phosphorylation in the SR region (Fig. 3A). The first of these mutants, S3D, altered the triplet S218–S220; the second, S4D, converted the same set of serines that were targeted in the S4A mutant (S197, S201, S205, and S209). Both the S3D and S4D mutations diminished the ability of N mRNA to boost gRNA infectivity (Fig. 3B), but to a more limited extent than was observed with the S4A mutant. When the same mutations were created in the MHV genome, the S3D mutant, like its S3A counterpart,

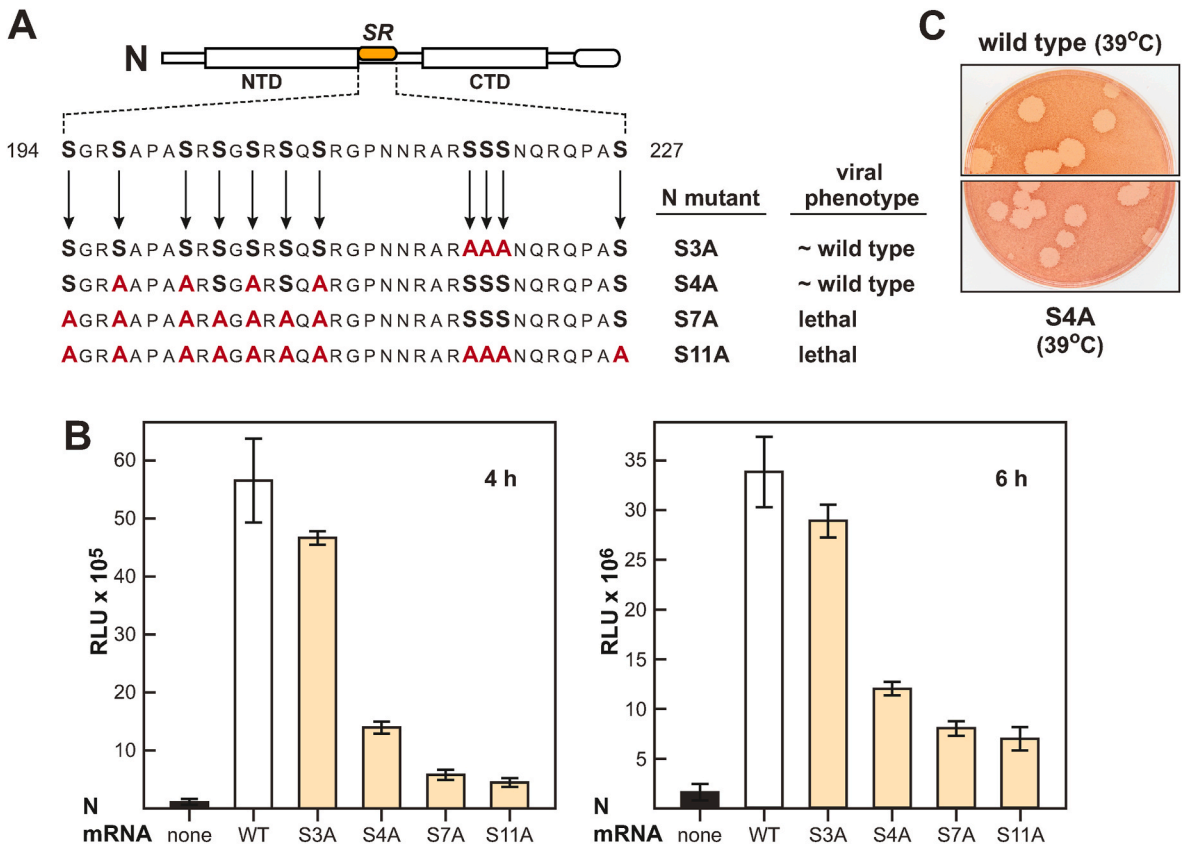

Fig. 2. SR region serine-to-alanine mutants. (A) Locations of serine-to-alanine SR mutations constructed in both N mRNA and viral mutants. Mutated amino acid residues are highlighted in red. (B) Stimulation of infectivity of GLuc-N[Alb1] gRNA at 4 h and 6 h post-transfection by mutant N mRNAs, compared to wild-type N mRNA. Each bar represents mean RLU (+/− standard deviation) from three separate transfections. (C) Plaques of the S4A viral mutant, compared to those of wild type at 39 °C, the temperature of the gRNA-mRNA cotransfection assay.

had an essentially wild-type phenotype. Unexpectedly, however, for the S4D mutant there was much greater divergence between the viral phenotype and the mRNA phenotype. Compared to the wild type, the S4D viral mutant formed small plaques at 37 °C and tiny plaques at 39 °C (Fig. 3C).

Two independent revertants were isolated from the S4D mutant. One of these had a second-site mutation, S61R, at the start of the NTD (Fig. 3A). The other exhibited a similar polar-to-basic change, N58K, at a nearby residue. Neither revertant contained any other mutation elsewhere in the N protein nor in the first 600 amino acids of nsp3 (an extent far beyond the Ubl1 and Ac regions). To test whether S61R was sufficient for reversion of the S4D phenotype, we reconstructed the S4D mutant containing this additional mutation. The resulting virus, S4Drev, formed plaques slightly smaller than wild-type plaques (Fig. 3C), confirming that a single NTD mutation could correct the deficiency caused by the set of serine-to-aspartate mutations in the SR region. However, there was no difference in the abilities of S4D and S4Drev N mRNAs to support gRNA infectivity (Fig. 3B), which again emphasized the lack of correspondence between the effects of the S4D mutations in cotransfection assays and in the viral genome. These results suggested that phosphorylation of the upstream serines in the SR region (S194–S209) modulates the N-nsp3 interaction early in infection, but maintenance of phosphorylation persistently throughout infection is extremely deleterious.

2.4. *Effects of arginine-to-alanine mutations in the SR region of N protein*

Arginines, the other salient constituents of the SR region, may provide an electrostatic counterbalance to negatively-charged phosphoserines and may also interact with RNA. We therefore created a set of mutants to examine the effects of removing these positively-charged residues by changing groups of them to alanines. One mutant, R3A, altered three arginine residues flanking the downstream serine triplet S218–S220 (Fig. 4A). A second mutant, R4A, knocked out four arginines adjacent to the upstream serines that were most profoundly affected in the S4A and S4D mutants (S197, S201, S205, and S209). Finally, the R7A mutant, encompassing all arginines in the SR region, combined the R3A and the R4A mutations. These mutations progressively decreased the capacity of N mRNA to stimulate gRNA infectivity in cotransfection assays, compared to the wild type (Fig. 4B). While R3A N mRNA was mildly attenuated, R4A N mRNA was markedly defective, and R7A N mRNA had still further reduced activity.

A corresponding decline in viral phenotype was obtained when the same mutations were introduced into the N gene in the MHV genome. The R3A mutant formed wild-type size plaques (Fig. 4C), but the R4A mutant was severely impaired, forming small plaques at 37 °C and tiny plaques at 39 °C (Fig. 4D). Consistent with the marginal viability of the R4A mutant, the R7A mutations were lethal. We isolated two independent revertants of the R4A mutant, both of which harbored second-site mutations. Remarkably, one of these had the same S61R mutation in the NTD that was shown to suppress the S4D mutations (Fig. 4A). The other revertant contained Q187R, located at the end of the NTD closest to the SR region. Neither revertant contained other mutations elsewhere in the N protein nor any changes in the first 600 amino acids of nsp3. Reconstruction of the R4A mutant with S61R showed that this single change was sufficient to reverse the R4A phenotype. The resulting virus, R4Arev, formed plaques that were smaller than those of the wild type but much larger than those of the original R4A mutant (Fig. 4D). Moreover, we found that the S61R mutation could even rescue the R7A mutant, albeit as a severely impaired virus. However, inclusion of the S61R mutation did not restore the ability of R4A N mRNA to enhance the

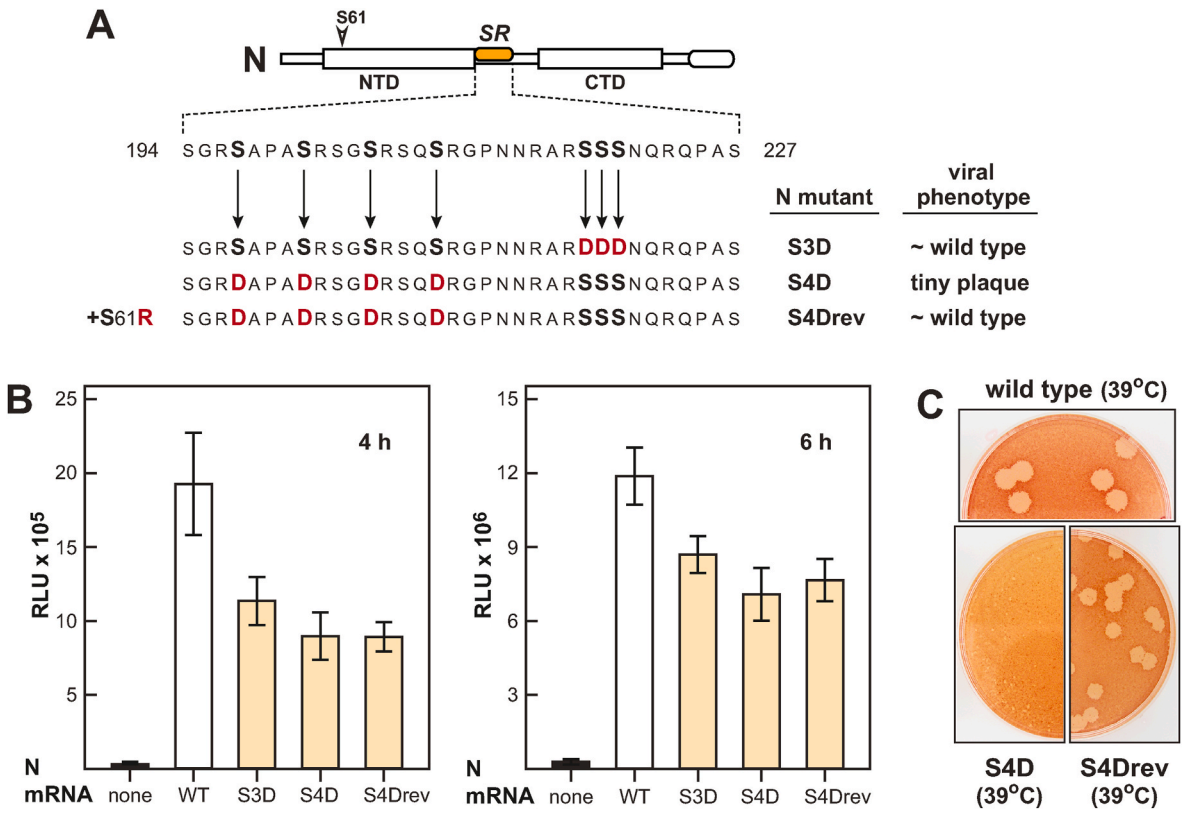

Fig. 3. SR region serine-to-aspartate mutants. (A) Locations of serine-to-aspartate SR mutations constructed in both N mRNA and viral mutants. Mutated amino acid residues are highlighted in red. Also shown is the location of S61, the NTD residue mutated in some viral revertants. (B) Stimulation of infectivity of GLuc-N[Alb1] gRNA at 4 h and 6 h post-transfection by mutant N mRNAs, compared to wild-type N mRNA. Each bar represents mean RLU (+/− standard deviation) from three separate transfections. (C) Plaques of the S4D and reconstructed S4Drev viral mutants, compared to those of wild type at 39 °C, the temperature of the gRNA-mRNA cotransfection assay.

infectivity of gRNA in cotransfection assays (Fig. 4E). This implied that, as with S4Drev, the early and the persistent effects of the reverting mutation differed.

Overall, the results shown in Figs. 2–4 indicate that altering combinations of charged residues (or transiently charged residues, as phosphoserines) in the SR region can reduce the ability of N mRNA to stimulate the infectivity of gRNA. In some cases, the extent of this attenuation is mirrored by viral phenotype. However, in other cases it cannot be directly correlated with viral phenotype, possibly pointing to additional functions of the N protein SR region in coordinating events during viral replication. Within the SR region, we observed that the upstream residues (S194–S209) appear to have the dominant role for enhancement of gRNA infectivity, which at least in part reflects the N-nsp3 interaction. Notably, none of the SR region mutations brought about an upregulation of N mRNA activity, relative to the wild type, in cotransfection assays. This supports the notion that phosphorylation is necessarily a dynamic process. Locking the phosphorylation status of serine residues, as in the S7A or S4D mutants, or abolishing the charge of adjacent residues, as in the R4A (and R7A) mutants, is consequently highly deleterious or lethal to the virus.

2.5. Pulldown of N protein SR region mutants by the Ubl1 domain of nsp3

To determine how the most broadly modified SR region mutants were affected in their interaction with nsp3, we performed pulldown assays with lysates from cells infected with these mutants. We and others had previously carried out pulldowns using GST fused to larger N-terminal segments of nsp3, which included the Ubl1 domain plus all (Hurst et al., 2010) or most (Cong et al., 2020) of the downstream Ac region. However, our subsequent genetic analysis (Hurst et al., 2013) as well as the biophysical study by Keane and Giedroc (2013) showed that the N-nsp3 interaction is confined solely to Ubl1. Therefore, in the current work we performed pulldowns with a GST-Ubl1 construct containing only the N-terminal 116 amino acids of nsp3. Additionally, for these experiments we used the reconstructed revertants of the most extensive serine-to-aspartate and arginine-to-alanine mutants in order to have sufficient N protein expression for our analysis.

GST-Ubl1, as well as control GST protein, was immobilized on glutathione affinity resin and then incubated with lysates from wild-type or mutant MHV-infected cells. As we observed previously, wild-type N protein was bound by GST-Ubl1, but not by GST alone (Fig. 5A). Also as noted previously, there was a marked increase of binding of wild-type N protein when the cell lysate was pretreated with RNase A (Fig. 5B). Lysates from cells infected with the S4A mutant behaved in the same fashion as the wild type. In contrast, binding of Ubl1 by N protein from lysates of cells infected with either the S4Drev mutant or the R4Arev mutant was already at this elevated level. Moreover, binding of these two mutant N proteins was not further enhanced by pretreatment with RNase A. This differential behavior of N protein from the wild type or the S4A mutant versus N protein from the S4Drev mutant or the R4Arev mutant suggests that there is a competition between RNA and Ubl1 for binding to the SR region of N protein. It has previously been noted that the N2a spacer (including the SR region) makes a contribution to RNA binding by N (Chang et al., 2009; Grossoehme et al., 2009). Our results could indicate that for wild-type N protein and the phosphorylation-restricted S4A N protein, optimal binding to Ubl1 can only be obtained following removal of RNA. On the other hand, the phosphomimic mutations in the S4D N protein or the ablation of positive charges in the R4A N protein likely weaken or eliminate RNA binding by the SR region, thereby allowing constitutive binding to Ubl1 without

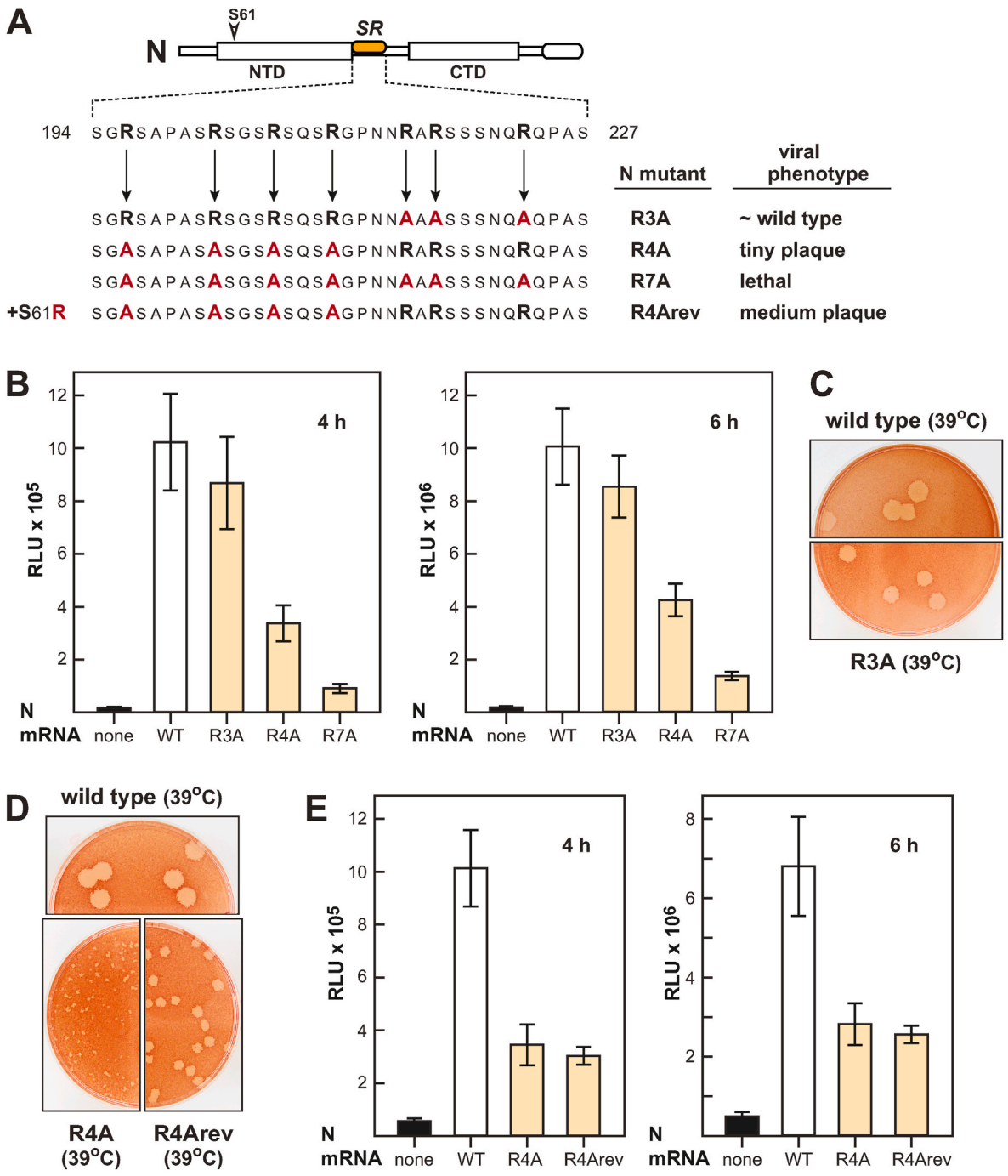

Fig. 4. SR region arginine-to-alanine mutants. (A) Locations of arginine-to-alanine SR mutations constructed in both N mRNA and viral mutants. Mutated amino acid residues are highlighted in red. Also shown is the location of S61, the NTD residue mutated in some viral revertants. (B and E) Stimulation of infectivity of GLuc-N [Alb1] gRNA at 4 h and 6 h post-transfection by mutant N mRNAs, compared to wild-type N mRNA. Each bar represents mean RLU (+/− standard deviation) from three separate transfections. (C) Plaques of the R3A viral mutant, compared to those of wild type at 39 °C, the temperature of the gRNA-mRNA cotransfection assay. (D) Plaques of the R4A and reconstructed R4Arev viral mutants, compared to those of wild type at 39 °C; wild-type plaques are the same as those shown in Fig. 3C.

RNase A pretreatment.

2.6. Mutational analysis of Ubl1

The Ubl1 domain is situated at the upstream end of the 2005-residue nsp3 protein of MHV (Fig. 6). Its amino terminus is created by the protease PLP1, a domain that is also contained within nsp3; a second internal protease domain, PLP2, processes the carboxy terminus of nsp3. Importantly, nsp3 is the first of three RTC subunits (the other two are nsp4 and nsp6) that become anchored to intracellular membranes and govern formation of the double-membrane vesicle compartments in which viral RNA synthesis occurs (Neuman, 2016; Snijder et al., 2020). To further define requirements of this interacting partner of N protein, we constructed mutants of Ubl1. We previously had constructed a set of mutants that changed surface clusters of charged amino acids to alanines, based on the positions of aligned MHV residues on the SARS-CoV Ubl1 structure (Serrano et al., 2007), with which it shares 35% sequence identity. Of these, Ubl1-mut1 and Ubl1-mut3 had wild-type-like phenotypes (Hurst et al., 2013). In contrast, Ubl1-mut2 was lethal, as was Ubl1-mut4, a deletion of most of Ubl1 (residues 19–111) that left the

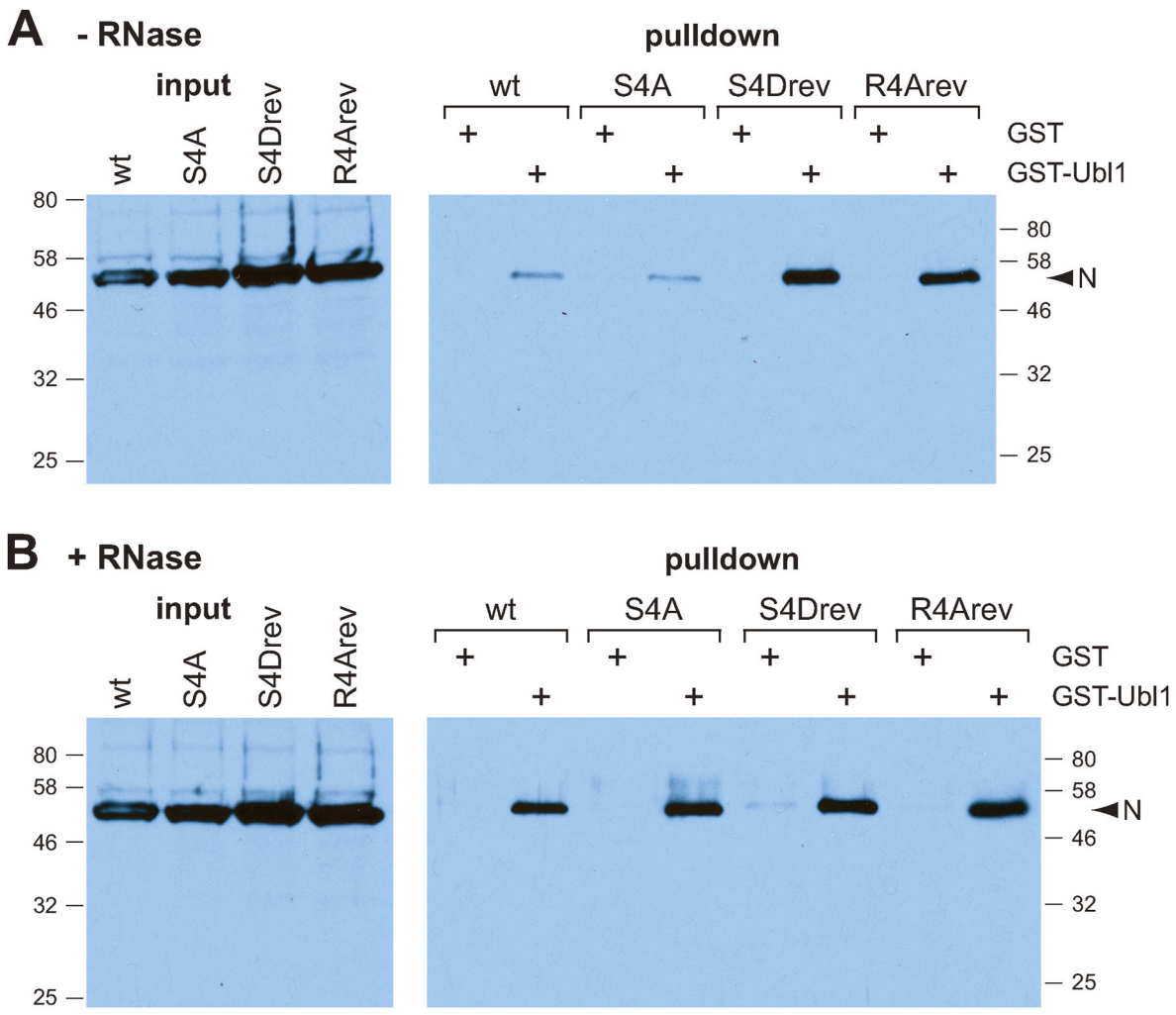

Fig. 5. Pulldown of wild-type and mutant N proteins by nsp3 Ubl1 domain. Bacterially expressed GST-Ubl1(1–116) fusion protein or GST alone were bound to glutathione affinity resin spin columns, as described previously (Hurst et al., 2010). Columns were incubated with lysates prepared from cells infected with wild-type MHV or with the S4A, S4Drev, or R4Arev mutants. Prior to binding, lysates were either (A) kept untreated or else (B) were pretreated by incubation with RNase A for 30 min at 37 °C. Bound proteins were eluted with glutathione, and equal amounts of eluted material were analyzed by Western blots probed with anti-N monoclonal antibody directed against an epitope in domain N3. There was no background signal with either GST-Ubl1 or GST for pulldowns with lysates from uninfected cells (data not shown). Molecular mass standards (kDa) are indicated for each panel.

nsp2-nsp3 cleavage site completely intact. The lethality of these latter two mutants demonstrated that the Ubl1 domain is an essential component of the coronavirus RTC.

With the availability of the structure of MHV Ubl1 (PDB 2M0A), we now focused on altering a ridge of negatively-charged residues formed by the α2 helix on one face of the molecule, which was reported to bind to a peptide corresponding to the MHV N SR region (Keane and Giedroc, 2013). The most extensive mutant created, Ubl1-mut5 (D51A, E52A, D55A, D59A, E62A), exhibited a severely defective phenotype, forming small plaques at 33 °C and 37 °C and very small plaques at 39 °C, relative to the wild type (Fig. 6). Moreover, stocks of this mutant had 10^3-fold lower titers than stocks of wild-type virus. Notably, two additional mutants, Ubl1-mut6 and Ubl1-mut7, each containing subsets of the Ubl1-mut5 mutations, had nearly wild-type phenotypes. This indicated that all five mutations in Ubl1-mut5 were necessary to produce its defect.

We isolated six independent revertants of Ubl1-mut5, all of which formed plaques comparable to those of the wild type (Fig. 6) and had regained the ability to grow to high titer. Sequencing of the nsp3 amino terminus of these revealed only two separate reverting mutations, both in the α2 helix of Ubl1. For two of the revertants, one of the original mutated residues of Ubl1-mut5 (E52A) had changed back to a different acidic amino acid, aspartate. The other four revertants retained the five original mutations of Ubl1-mut5 and added one further mutation, L54R, among them. This was somewhat perplexing, since these revertants not only preserved the loss of all of the negative charges in the α2 helix but also introduced a positive charge. However, leucine-54 is buried in the native structure of MHV Ubl1 (PDB 2M0A), and it is possible that its replacement by arginine could significantly alter the conformation of Ubl1, thereby increasing the accessibility of other surfaces of this domain that participate in contacts with the SR region and the NTD of N protein. To further determine whether the observed mutations in Ubl1 were responsible for both the original lesion and for reversion, we sequenced the entire N gene of all revertants, and all were found to have the wild-type sequence. Additionally, whole genome sequencing was carried out on Ubl1-mut5 and on representatives of each class of revertant, Ubl1-mut5-rev1 and Ubl1-mut5-rev2. This analysis confirmed the already noted mutations in Ubl1, and there were no extraneous mutations except for a single coding mutation, P1241H, in nsp3 of the original Ubl1-mut5 isolate and both revertants. Since that mutation occurred in the genomes of all three viruses and fell in a hypervariable region between the NAB and G2M domains of nsp3, we deemed it to not be relevant. The confirmation that single mutations within Ubl1, A52D and L54R, fully account for reversion of Ubl1-mut5 argues that the

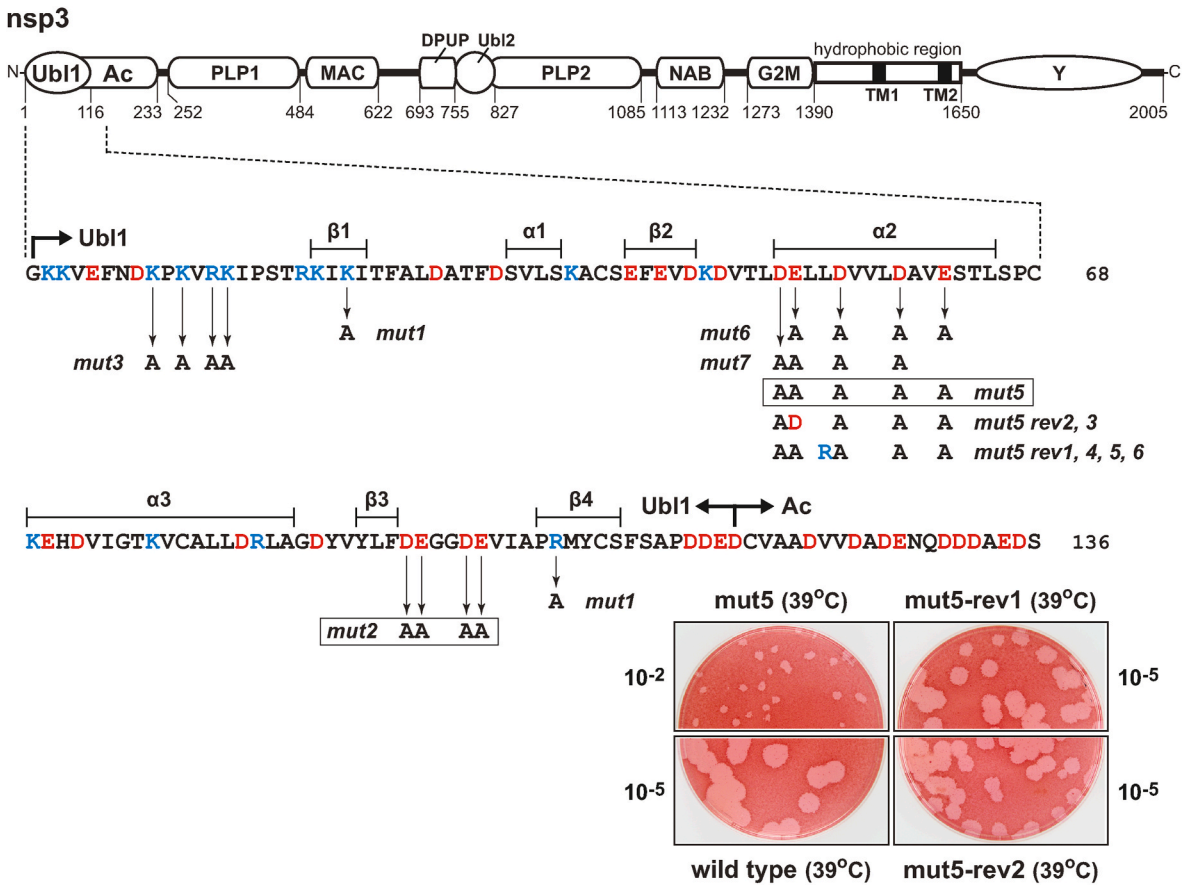

Fig. 6. Ubl1 mutants. A schematic of MHV nsp3 is shown at the top, with amino-acid residues numbered; the first amino acid of mature nsp3 is residue 833 of the unprocessed replicase polyprotein. Nomenclature for the domains of nsp3 is mostly that of Neuman and coworkers (Neuman et al., 2008; Neuman, 2016): *Ubl*, ubiquitin-like domain; *Ac*, acidic region; *PLP*, papain-like protease; *MAC*, macrodomain; *DPUP*, domain preceding Ubl2 and PLP2 (Chen et al., 2015); *NAB*, nucleic acid binding domain; *G2M*, coronavirus group 2 (now betacoronavirus) marker domain; *TM*, transmembrane segment; *Y*, coronavirus highly conserved domain. Beneath is shown the sequence of Ubl1 and a small segment of the adjacent Ac region; acidic and basic amino acids are highlighted in red and blue, respectively. The loci of mutants mut1-mut3 and mut5-mut7, as well as revertants of mut5, are indicated below the sequence. Mutants with significant phenotypes are boxed: mut2 is lethal; mut5 forms very small plaques at 39 °C. An additional mutant, mut4, deleting amino acids 19–111, is also lethal. Mutants mut1-mut4 have been reported previously (Hurst et al., 2013); mut5-mut7 were created in the current study. Plaques of mut5 and two of its revertants, compared to those of the wild type at 39 °C, are shown at the bottom; the dilution of virus stock is indicated beside each plaque titration.

phenotype of this mutant is meaningful and strongly suggests that it is defective in interaction with some other viral component. However, we were not able to identify any revertants containing second-site mutations in the N gene.

2.7. Construction of a SARS-CoV N protein - Ubl1 chimera

Since the N-nsp3 interaction had first been revealed by replacement of the MHV N protein with the closely related BCoV N protein, we next sought to extend this approach across a greater phylogenetic distance, using the SARS-CoV N protein. We previously found that the MHV N protein well tolerated substitution of either the NTD or the CTD from SARS-CoV N protein, but we could not substitute both domains simultaneously (Kuo et al., 2014). Moreover, as noted above, substitution in MHV of the SR region from the SARS-CoV N protein was lethal unless accompanied by reverting mutations in both the SR region and Ubl1 (Hurst et al., 2010). We therefore set out to exchange nearly the entire MHV N protein as well as the Ubl1 domain of nsp3 with their SARS-CoV counterparts. Accordingly, we designed a chimera, designated Ubl1/N (SARS-CoV) containing: (i) amino acids 4–116 of MHV Ubl1 replaced by the corresponding amino acids 6–114 of SARS-CoV Ubl1; and (ii) amino acids 1–379 of MHV N replaced by amino acids 1–361 of SARS-CoV N (Fig. 7A). The first substitution kept the initial three residues of MHV Ubl1 to ensure correct processing of the nsp2-nsp3 junction. The latter substitution encompassed all domains of N, except for the carboxy-terminal spacer B and domain N3, which were retained in order to preserve the specific and essential interaction of N with the MHV M protein (Kuo et al., 2016). Ubl1/N(SARS-CoV) was obtained by two stages of targeted RNA recombination. First, the previously constructed Ubl1(SARS-CoV) mutant (Hurst et al., 2013) was recombined with donor RNA containing the feline coronavirus spike glycoprotein gene to generate fMHV-Ubl1(SARS-CoV), a counterpart to fMHV.v2 (Goebel et al., 2004), which was selected on feline cells. Then fMHV-Ubl1 (SARS-CoV) was used as the recipient virus in targeted RNA recombination with donor RNA containing the N(SARS-CoV) substitution, and selection was carried out on murine cells. In this manner, we recovered four independent isolates of Ubl1/N(SARS-CoV). Conversely, numerous independent targeted RNA recombination experiments using fMHV.v2 as the recipient virus with N(SARS-CoV) donor RNA did not yield any progeny. This showed that, consistent with our expectations, the N (SARS-CoV) substitution was lethal unless accompanied by the Ubl1 (SARS-CoV) substitution.

All isolates of the Ubl1/N(SARS-CoV) chimera had the same phenotype, forming plaques at 33 °C and 37 °C that were smaller, and at 39 °C much smaller, than those of the wild type (Fig. 7B).

This suggested that, despite accommodating all known N-nsp3 and N-M interactions, this mutant was partially impaired. To probe the basis for this defect, we obtained fifteen independent Ubl1/N(SARS-CoV)

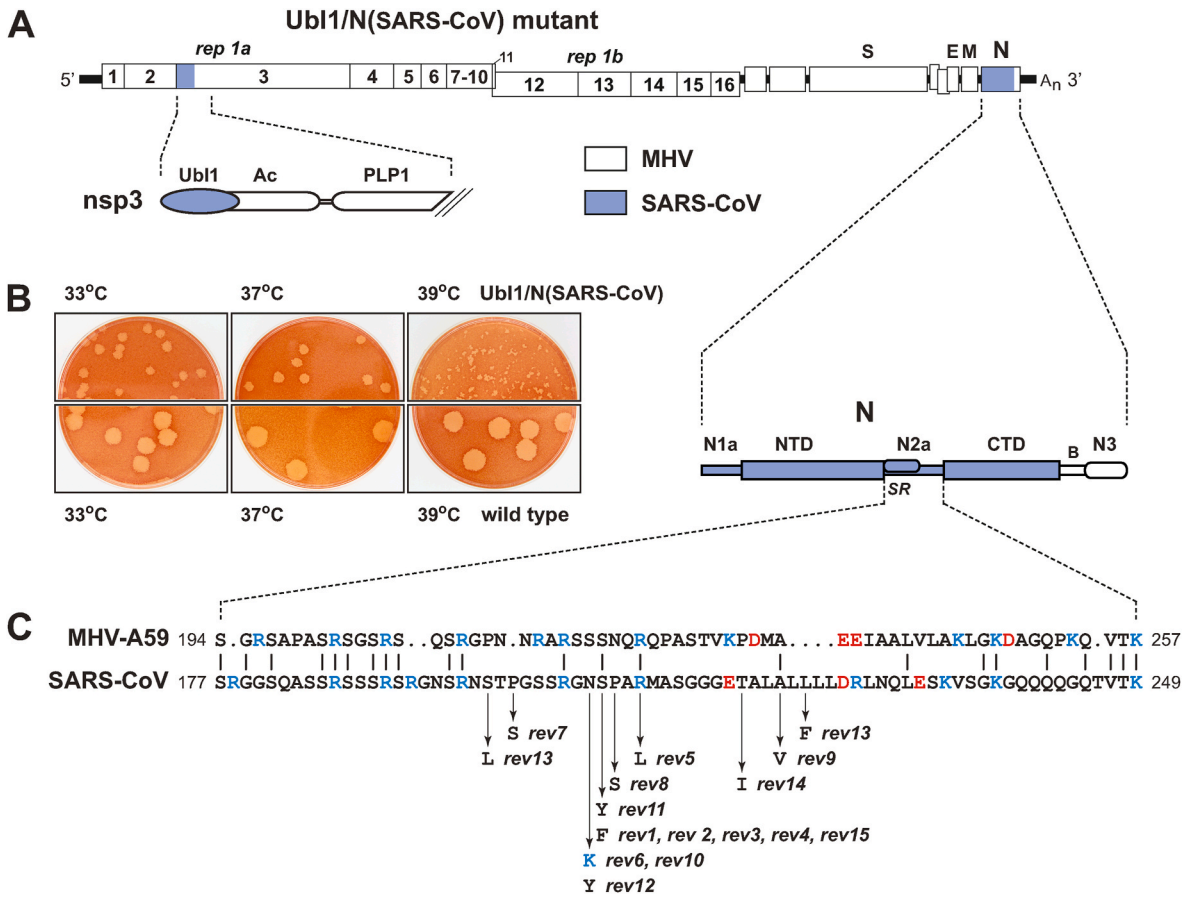

Fig. 7. Chimeric MHV mutant containing N protein and Ubl1 from SARS-CoV.
(A) Schematic of the MHV genome, with expanded segments of the nsp3 and N genes showing substitutions made from the SARS-CoV genome. In the encoded proteins, residues 4–116 of MHV Ubl1 were replaced by residues 6–114 of SARS-CoV Ubl1; residues 1–379 of MHV N were replaced by residues 1–361 of SARS-CoV N. (B) Plaques of the Ubl1/N(SARS-CoV) mutant, compared to those of wild-type MHV at 33, 37, and 39 °C. (C) Aligned sequences of the N2a segments of the MHV and SARS-CoV N proteins; acidic and basic amino acids are highlighted in red and blue, respectively. Beneath the SARS-CoV sequence are shown the loci of mutations found in 15 independent revertants of the Ubl1/N(SARS-CoV) mutant. One additional mutation in the NTD, P81L, was contained in both rev10 and rev13.

revertants (five from each of three separate isolates). These were isolated following serial passages at 39 °C of multiple individual cultures, each of which had been started from a single plaque of Ubl1/N(SARS-CoV). The revertants formed plaques at 39 °C that were markedly larger than those of the original chimera but were not fully as large as wild-type plaques. To determine the mutations that had been acquired, the entire M and N genes of all revertants were sequenced. In almost all cases, each revertant had only a single mutation, which fell in the N2a spacer between the NTD and the CTD of N protein (Fig. 7C). The only two exceptions to this pattern were rev10, which had an additional mutation (P81L) in the NTD, and rev13, which had two mutations in the N2a segment plus the same NTD mutation as rev10. No mutations were found elsewhere in the N protein or the M protein. Whole genome sequencing was also carried out on a subset of the revertants: rev4, rev8, rev9, rev14, and rev15. This revealed only two additional coding mutations. The first of these, I370V in nsp13, occurred in all five revertants and also in the three original Ubl1/N(SARS-CoV) isolates that were sequenced, and it was thus not considered relevant. The second, A30V in nsp13 was found only in rev9; however, since it was located at a position that is conserved in nsp13 of all betacoronaviruses, its significance cannot be ruled out at this time. Strikingly, then, nearly all of the reverting mutations mapped in the N2a spacer segment and were located downstream of the SR region, separate from the loci of the original BCoV N revertants (Hurst et al., 2010). The MHV and SARS-CoV N proteins have only 32% overall sequence identity in the N2a linker (Fig. 7C), but none of the revertants changed a SARS-CoV amino acid to its MHV counterpart. Since the Ubl1/N(SARS-CoV) chimera paired the N protein with its cognate Ubl1 partner, it is not clear what defect was remedied by the revertants. Our results and those of Cong et al. (2020) make it unlikely that an as yet unidentified nsp interacts with N. Thus, our data may indicate that the N2a region contributes to an interaction between N protein and viral RNA sequences or structures that are different between MHV and SARS-CoV.

3. Discussion

3.1. Characterization of the N-nsp3 interaction

The results presented here emphasize the critical nature of the interaction between the coronavirus N protein and the nsp3 subunit of the viral RTC. This intermolecular association, principally mediated by the N2a spacer of N and the amino-terminal Ubl1 domain of nsp3, is essential for the efficient initiation of infection by gRNA. To more directly monitor the infectivity of transfected MHV gRNA, we developed a reporter virus, GLuc-N[Alb1], which provided a quantitative readout of viral replication via assay of secreted luciferase activity (Fig. 1D). The

GLuc-N[Alb1] genome also included the defective N gene from the Alb1 MHV mutant (Masters et al., 1994) in order to forestall autologous stimulation of gRNA infectivity by its own encoded N protein. This allowed us to examine the ability of constructed N mutants to boost gRNA infectivity in a system in which cotransfected N mRNA was effectively the only source of N protein early in infection.

Our mutational analyses focused on the SR region that occupies the upstream half of the N2a spacer, since previous studies pointed to this as the main nsp3-interacting segment of N protein (Hurst et al., 2010, 2013; Keane and Giedroc, 2013). Although all coronavirus N proteins contain SR regions, they exhibit little sequence conservation, even among closely-related coronaviruses, such as MHV and BCoV; across coronavirus subgenera or genera they diverge even more extensively, both in sequence and size. Thus, phylogenetic comparisons do not offer up conserved amino acid residues as candidates for mutagenesis. Notably, the SR region is a major locus of N protein phosphorylation by host protein kinases (Peng et al., 2008; Davidson et al., 2020; Bouhaddou et al., 2020), and our targeting of mutations was influenced in part by a report that implicated GSK-3 as the relevant kinase acting on MHV N (Wu et al., 2009). We constructed mutants containing multiple serine-to-alanine (Fig. 2) or serine-to-aspartate mutations (Fig. 3) to progressively prevent or mimic phosphorylation, respectively. Similarly, mutants with multiple arginine-to-alanine mutations (Fig. 4) were created to progressively reduce the concentration of positive charges in the SR region. This strategy revealed that, although no individual residue in the SR region is critical, the grouping of sets of each type of mutation had a cumulative inhibitory effect on the ability of N mRNA to stimulate gRNA infectivity. In this respect, our results may parallel those of Cong et al. (2020), who observed that certain clusters of multiple mutations in spacer N2a abolished in vitro binding to $nsp3^N$; additionally, those investigators saw a separate contribution of the NTD, which our work did not directly address. However, evidence for participation of the NTD in $nsp3^N$ binding was also detected in the study by Keane and Giedroc (2013), and it may be implied by our finding of second-site NTD mutations that suppressed the most severely defective SR region serine-to-aspartate and arginine-to-alanine mutants.

We found that the progressive aggregation of each type of serine or arginine substitution led to a stepwise reduction of the activity of N mRNA in cotransfections with gRNA. The extent of this inhibition was often, but not always, matched by the phenotypes of viral mutants constructed with the same N mutations, which ranged from nearly wild-type to tiny-plaque to lethal. The lack of an exact correspondence between the two systems was probably because one measures the transient effect of particular sets of mutations on the launch of infection, while the other determines the persistent effects of those same mutations on all phases of viral infection. The main conclusion we draw from these results is that serine phosphorylation, in conjunction with the constellation of positively-charged arginine residues, acts as a dynamic switch regulating the binding of N protein to Ubl1 and probably also to RNA. Multiples of any of the types of mutation – serine-to-alanine, serine-to-aspartate, or arginine-to-alanine – permanently engage the switch in one position, either preventing the N-Ubl1 interaction or else inhibiting its dissociation. Both of these outcomes are harmful or lethal for the virus. This view is supported by our examination of the effects of RNase treatment on GST-Ubl1 pulldown of N protein from lysates of cells infected with wild-type or mutant MHV (Fig. 5). We found that binding of wild-type or S4A N protein to Ubl1 was markedly enhanced by prior digestion of RNA in lysates, indicating that there is a competition between RNA and Ubl1 for binding to the SR region. Contrary to this, Ubl1 binding by the S4D or R4A N proteins was already at an elevated level that was not affected by RNase, suggesting that the altered SR regions of these mutant N proteins have a reduced affinity for RNA, allowing its easy displacement by Ubl1. We previously pointed out the RNase-induced enhancement of GST-Ubl1 pulldown of wild-type N protein (Hurst et al., 2010). Similarly, Keane and Giedroc (2013) found that high-affinity binding to Ubl1 was abolished when a wild-type NTD-SR construct was pre-bound to RNA. In contrast, Cong and coworkers did not observe an increased pulldown of N protein following RNase treatment of lysates of cells infected with wild-type MHV (Cong et al., 2020). We note, however, that they performed RNase A incubations on ice, whereas ours were carried out at 37 °C and thus were likely more extensive.

To complement our study of the N protein SR region, we carried out two further genetic analyses. In the first, we constructed a set of Ubl1 mutants ablating acidic residues in a helix that had been shown by NMR to form the principal contact with the SR region (Keane and Giedroc, 2013). Only the most extensive of these mutants, Ubl1-mut-5, which changed five aspartates and glutamates to alanines, displayed a distinctly defective phenotype (Fig. 6). Together with previously created nsp3 mutants (Hurst et al., 2013), this confirmed the essential nature of Ubl1. This result also echoed our experience with mutagenesis of the SR region, where the most significant effects were seen only upon accumulation of multiple mutations. Paradoxically, the most commonly arising reverting mutation for Ubl1-mut5 introduced a positive charge into the helix that had already been stripped of all negative charges. This finding indicates that binding of N to Ubl1 is not solely governed by electrostatic interactions, but that conformational changes likely also come into play. In the same manner, phosphorylation of the N SR region may affect its structure as well as its pattern of charge, as it has been demonstrated that phosphorylation can regulate a disordered-to-folded transition of a protein (Bah et al., 2015). In the second genetic analysis, we constructed a chimera in which the SARS-CoV N protein entirely replaced that of MHV, except for the carboxy-terminal domain N3, which is necessary for N protein to assemble with its corresponding (MHV) M protein. The resulting chimeric virus, Ubl1/N(SARS-CoV) (Fig. 7), could only be recovered if the MHV Ubl1 domain was also replaced by its SARS-CoV counterpart, reinforcing our expectation that SCoV N protein had to interact with its cognate Ubl1. However, the chimera was not as fit as wild-type MHV, prompting us to isolate a large set of independent revertants. All reverting mutations mapped to the N protein and, almost exclusively, to spacer N2a (except for two revertants in which an additional mutation occurred in the NTD). However, the Ubl1/N(SARS-CoV) reverting mutations fell further downstream of where the BCoV N substitution reverting mutations had localized (Hurst et al., 2010) and were mostly distal to the SR region. The absence of reverting mutations anywhere else in the viral genome other than the coding region for the N2a spacer raises the possibility that N2a contributes to the recognition of viral RNA sequences or structures that differ between MHV and SARS-CoV.

3.2. Role of the N-nsp3 interaction

We previously proposed that the N-Ubl1 interaction serves at the outset of infection to tether the viral gRNA to the newly translated coronavirus RNA synthesis machinery, the RTC (Hurst et al., 2010, 2013). Such an attachment would thereby coordinate the dual functions of gRNA, which acts first as an mRNA and then as the initial template for RNA synthesis. Although N protein is displaced from the 5′ two-thirds of incoming gRNA during translation of the RTC, retained nucleocapsid structure at the 3′ end of the genome would allow its immediate association with nsp3, which is the first membrane-anchored translation product. This model was consistent with the observed colocalization of N and replicase components (van der Meer et al., 1999; Sims et al., 2000; Stertz et al., 2007; Ulasli et al., 2010). Additionally, the assistance of N in the formation of the initiation complex at the 3′ end of gRNA would explain how N could stimulate both transcription and genome replication (Thiel et al., 2001; Schelle et al., 2005; Almazán et al., 2004; Zúñiga et al., 2010).

This hypothesis must now be revised in light of remarkable new advances that have been made in the visualization of intracellular compartments that form during infection. Numerous remodeled membranous structures have been observed in coronavirus-infected cells,

including double-membrane vesicles (DMVs), convoluted membranes, zippered endoplasmic reticulum (ER), and double-membrane spherules, some of which originally appeared to be specific to particular viruses in the family (Knoops et al., 2008; Ulasli et al., 2010; Maier et al., 2013; Neuman, 2016). However, a systematic ultrastructural analysis found that, across all coronavirus genera, essentially the same types of ER-derived structures are induced by infection (Snijder et al., 2020). Most importantly, it was shown by direct metabolic labeling and EM autoradiography that the primary site of viral RNA synthesis is the interior of DMVs. DMVs are among the earliest detected structures following infection (Ulasli et al., 2010; Mihelc et al., 2021). They are approximately spherical vesicles, with average diameters of 200–300 nm, surrounded by closely paired membrane bilayers. DMVs were previously associated with active RNA synthesis because they harbor abundant double-stranded RNA, an intermediate in the production of both gRNA and sgRNA, as well as various nsp components of the RTC. Notably, there are no ribosomes located in the interior of DMVs, which suggests that these organelles do not simply form around the replicase polyprotein as it is being translated and processed. Significantly, DMVs do not have detectable openings to the cytoplasm (Knoops et al., 2008; Maier et al., 2013; Snijder et al., 2020; Mihelc et al., 2021). Their closed nature thus posed the problem of how RNA precursors and products are able to traffic between the DMV interior and the cytoplasm (Fig. 8).

A surprising solution to this problem was very recently revealed by a high-resolution cryo-electron tomographic study that imaged DMVs in MHV-infected cells (Wolff et al., 2020). This work showed that nsp3 is the major constituent of a molecular pore that spans both membrane bilayers of the DMV, connecting the interior space to the cytoplasm. The pore structure is hexameric, with a crown-like external face sitting on a platform embedded in the membrane. Strikingly, it was found that the Ubl1 domains of each of the six nsp3 monomers are situated on the exterior of the DMV, projecting into the cytoplasm as the points of the crown (Fig. 8B and C). The channel formed by this structure is some 6 nm in diameter in the DMV interior, narrowing to 2–3 nm on the cytoplasmic surface. An opening of this size could accommodate a strand of RNA, but it would be too narrow for passage of the viral nucleocapsid (Klein et al., 2020; Yao et al., 2020) or even free N protein dimers (Gui et al., 2017).

Crucially, the topology of the pore indicates that N protein molecules that are bound to Ubl1 are on the opposite side of the DMV double membrane from where viral RNA synthesis takes place. This circumstance brings into finer focus the nature of the recruitment of N protein to the site of RNA synthesis. Although N has been shown to localize in the vicinity of DMVs and other membranous structures, it has never been clearly observed in the interior of DMVs (Stertz et al., 2007; Ulasli et al., 2010: Snijder et al., 2020). Indeed, most currently available evidence indicates that N protein is solely located in the cytoplasm outside of DMVs, suggesting that it could not directly interact with the enzymatic components of RNA synthesis. This is also supported by the Y2H analysis of Cong et al. (2020), which showed that nsp3 is the only one of the 16 RTC subunits that interacts with N protein. Thus, the results presented here and previously (Hurst et al., 2010, 2013; Cong et al., 2020) prompt us to conclude that the predominant role of the N-nsp3 interaction is in the initiation of infection. This would explain why N protein is required for the successful launch of infection from gRNA and why N mutations that impair the N-nsp3 interaction are deleterious to the virus. We therefore propose that N stimulates RNA synthesis by enabling the initial entry of gRNA into the DMV at the outset of infection (Fig. 8B). This

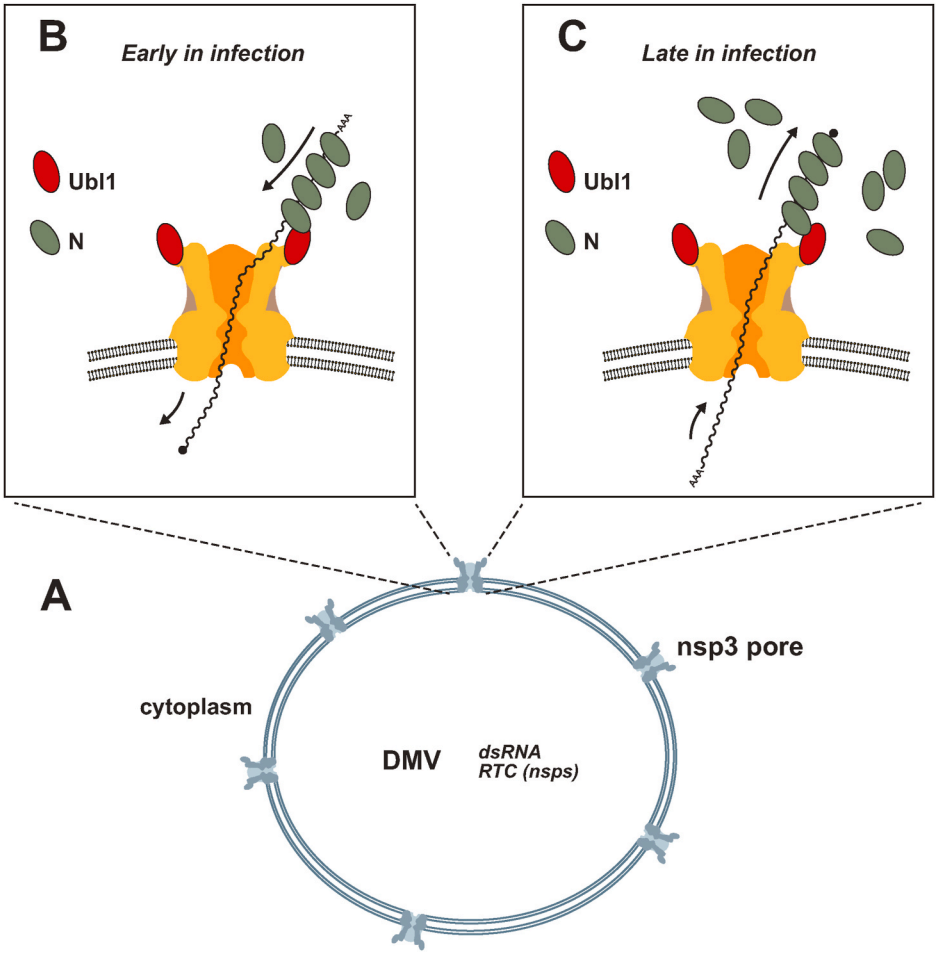

Fig. 8. Framework for delineating the role of the N-nsp3 interaction in coronavirus RNA synthesis. (A) Schematic of the newly discovered molecular pore in the double-membrane vesicle (DMV), formed principally by nsp3 (Wolff et al., 2020). The hexameric pore, which is present in multiple copies, spans the two membrane bilayers and connects the DMV interior to the cytoplasm. The Ubl1 domains of each nsp3 monomer project from the cytoplasmic face of the structure. The central channel of the pore is large enough to accommodate passage of RNA strands, as well as the passive import of RNA precursors and metabolites. (B) Proposed role of the N-Ubl1 complex in the initiation of infection. Successive cycles of Ubl1 interaction with N protein monomers bound to the distal end of the genome would bring about delivery of the previously translated gRNA to the interior of the DMV to serve as the substrate for the replicase-transcriptase complex (RTC). (C) At later stages of infection, N associated with Ubl1 may also participate in the export of sgRNA and progeny gRNA molecules from the DMV to the cytoplasm.

could come about through successive cycles of N alternately binding to Ubl1 or to gRNA, as governed by phosphorylation and dephosphorylation. The RNA chaperone activity that has been demonstrated for the coronavirus N protein (Zúñiga et al., 2010) may play a role in this process by maintaining the long gRNA molecule in a disentangled state to allow it to thread through the pore. Additionally, other domains of nsp3, many of which possess general RNA-binding activity could contribute to translocation of the genome (Neuman, 2016). At subsequent stages of infection, once active RNA synthesis has been established, N bound to Ubl1 may also act to facilitate the exit to the cytoplasm of sgRNAs for translation and progeny gRNA molecules for encapsidation and assembly (Fig. 8C). Much further investigation will be required to advance this speculative framework to a fully developed mechanism. One exciting avenue to pursue would be the elucidation of what other viral and cellular factors are associated with the separate faces of the newly discovered DMV pore.

4. Materials and methods

4.1. Cells and viruses

MHV strain A59 wild type and mutants were grown in mouse 17 clone 1 (17Cl1) cells. Plaque titrations and plaque purifications were carried out with mouse L2 cells. Plaques shown were visualized by staining with neutral red at 72 h postinfection and were photographed 18 h later. Both murine cell lines were maintained in monolayer in Dulbecco's modified minimal essential medium (DMEM) containing 10% fetal bovine serum. Spinner cultures of L2 cells were maintained at densities between 1 x 10^5 and 2 x 10^6 cells/ml in Joklik's MEM containing 10% fetal bovine serum. The host-range chimeric coronavirus designated fMHV.v2 (Goebel et al., 2004) was propagated in feline FCWF cells that were maintained in low-glucose DMEM containing 10% fetal bovine serum.

4.2. MHV mutant construction

MHV N gene mutants and the GLuc-N[Alb1] reporter mutant were created by targeted RNA recombination, which has been described in detail elsewhere (Goebel et al., 2004). Briefly, in this method feline cells were infected with fMHV.v2, which carries the feline coronavirus spike (S) protein, and were then transfected with synthetic donor RNA restoring the MHV S gene and the mutations of interest. Mutant recombinants were then selected based on recovery of the ability to grow in mouse cells. Particular sets of constructed mutations were judged to be lethal if they yielded no recombinants in multiple targeted RNA recombination trials in which side-by-side positive controls with wild-type donor RNA produced recombinants at a high frequency. The two-step isolation of the chimeric virus Ubl1/N(SARS-CoV) by targeted RNA recombination is described in Results. RTC subunit nsp3 mutants Ubl1-mut5, Ubl1-mut6, and Ubl1-mut7 were generated by in vitro assembly and transcription of full-length MHV cDNA using the system devised by the Baric laboratory (Yount et al., 2002). Mutant viruses were recovered by transfection of L2 cells with synthetic gRNA augmented with synthetic MHV N mRNA.

All viral mutants were purified by plaque titration and RNA was extracted from first passage-infected cells with Ultraspec reagent (Biotecx). To confirm the composition of constructed mutants, reverse transcription (RT) of RNA was carried out with random hexanucleotide primer and avian myeloblastosis virus reverse transcriptase (Life Sciences). PCR amplification of cDNA was performed with the Expand High Fidelity PCR System (Roche), and RT-PCR products were purified with QIAquick spin columns (Qiagen) prior to Sanger DNA sequencing. The presence of constructed mutations, as well as the absence of extraneous mutations, was verified through sequencing of the entire N gene, at least parts of the adjacent M gene and 3′ UTR, and the region of gene 1 encoding the first 600 amino acids of nsp3. In the case of the GLuc-N[Alb1] mutant the entire gene 4 substitution was also confirmed.

For constructed mutants with significantly defective phenotypes, independent revertants were obtained from cultures, each of which was started from a single separate plaque of a given mutant. Cultures were passaged three to six times at 39 °C, by which time accelerated growth was usually noted, and plaque titrations were then carried out at 39 °C. A single large plaque originating from each culture was purified for further analysis. The extent of Sanger sequencing of revertant viruses is indicated in Results. For whole genome sequencing of some Ubl1-mut5 and Ubl1/N(SARS-CoV) revertants, tagged libraries were prepared with a Nextera XT kit (Illumina) from overlapping 1.0–2.5 kb RT-PCR amplicons spanning the MHV genome and were sequenced on a MiSeq Sequencer (Illumina). Viral genome sequences were fully assembled using SPAdes version 3.0.0 with the read correction mode active and K-mer sizes of 21, 33, 55, 77, 99, and 127.

4.3. Plasmid construction

N gene mutants (S3A, S4A, S7A, S11A, S3D, S4D, R3A, R4A, and R7A) were constructed by standard techniques initially in plasmid pCK70XB (Hurst et al., 2013), which is a transcription vector for wild-type MHV sgRNA7, the mRNA for N protein. This plasmid harbors a unique coding-silent *Psp*XI site within N gene codons 14–16 and a unique coding-silent *Bsp*EI site within codons 444–446. For the generation of corresponding transcription vectors for donor RNA used in targeted RNA recombination, each *Psp*XI-*Bsp*EI fragment was then shuttled into pSG6X (Kuo et al., 2014), which contains the 3′-most 8.6 kb of the MHV-A59 genome. Similarly, transcription vector pSG-lucA1, the donor RNA template for the GLuc-N[Alb1] mutant, was made by replacement of the *Sal*I-*Not*I fragment of an earlier gene 4 substitution, pG1-Nd3 (Hurst et al., 2009), with a PCR-generated *Xho*I-*Eag*I fragment containing the *Gaussia princeps* luciferase gene from pCMV-GLuc (New England Biolabs). The Alb1 N gene mutations (Masters et al., 1994) were then transferred into this plasmid from a pCK70XB-based vector harboring the L123R and W126C mutations.

The Ubl1-mut5, Ubl1-mut6, and Ubl1-mut7 mutations were constructed in pA3B2 (Hurst et al., 2013), a derivative of clone A of the infectious cDNA system of Yount et al. (2002), by replacement of the *Xba*I-*Sal*I fragment with fragments synthesized by PCR from overlapping oligonucleotides. Transcription vector pMN14, the donor RNA template for the Ubl1/N(SARS-CoV) mutant, was constructed via multiple intermediates from segments obtained from previously described chimeric plasmids (Kuo et al., 2016) plus fragments that were generated through PCR or two-step PCR using a cloned SARS-CoV N gene cDNA as the template (strain Urbani; GenBank accession number AY278741). The overall compositions of constructed plasmids were confirmed by restriction analysis, and all ligation junctions and regions generated by PCR amplification were verified by DNA sequencing. Oligonucleotides for PCR and DNA sequencing were from Integrated DNA Technologies.

4.4. Assay for gRNA - N mRNA cotransfection

Preparation and cotransfection of gRNA and N mRNA were exactly as described in detail previously (Hurst et al., 2013). In brief, gRNA was isolated from highly purified virions of GLuc-N[Alb1] by phenol-chloroform extraction and ethanol precipitation. Wild-type and mutant N mRNAs were synthesized in vitro from *Hind*III-linearized pCK70XB-derived vectors with a mMessage mMachine T7 kit (Ambion); following template removal with DNaseI, mRNAs were purified on spin columns and integrity was monitored by agarose gel electrophoresis. Isolated gRNA and mRNAs were finally resuspended in water and quantitated by A_{260}. Mixtures of gRNA (0.25 μg/sample) and mRNA (0.50 μg/sample), or water control, were electroporated into 5 x 10^6 L2 cells, which had been grown in suspension culture, by two consecutive pulses from a Bio-Rad Gene Pulser II apparatus set at 0.3 kV and 975 μF. (Optimal amounts of each RNA had been determined in preliminary

experiments.) Transfected cells were then diluted with 1.8 x 10^6 fresh L2 cells, and the cell mixture was seeded into one 10-cm^2 well of a six-well plate. Following 3 h at 39 °C to allow for attachment and recovery, the medium was replaced, incubation at 39 °C was resumed, and 100 μl aliquots of medium were withdrawn at the indicated times. Secreted luciferase expression was measured with a BioLux Gaussia luciferase assay kit (New England Biolabs), and relative light units (RLU) were read in a Promega Glomax luminometer.

4.5. GST-Ubl1 pulldown assay

Procedures for GST-Ubl1 pulldown were carried out essentially identically as described in detail previously (Hurst et al., 2010). Plasmid pGEX6P-Ubl1, for expression of a GST fusion of only the Ubl1 domain of nsp3, was constructed by replacement of the *Ava*I-*Eag*I fragment of pGEX6P-nsp3(1–273) with an oligonucleotide cassette that created two tandem stop codons following codon 116 of nsp3 (the downstream boundary of Ubl1). Bacterial lysates were prepared from *E. coli* Rosetta pLysS cells (Novagen) transformed with pGEX6P-Ubl1, or the control pGEX6P (Pharmacia), following induction with 1 mM IPTG at 20 °C for 18 h. Lysates of 17Cl1 cells infected at 37 °C with wild-type MHV or the S4A, S4Drev, or R4Arev mutants were prepared at 9 h after infection of nearly confluent monolayers at a multiplicity of 4 PFU per cell; control mock-infected lysates were generated identically. Treatment of lysates with RNaseA for 30 min at 37 °C was exactly as described previously (Hurst et al., 2010). The amount of N protein in infected cell lysates was determined by Western blot quantitated with a ChemiDoc XRS + imager (Bio-Rad), and lysates were then normalized to contain equal amounts of N by addition of mock-infected lysate. GST pulldown assays were carried out with glutathione affinity resin, spin columns, and associated reagents obtained from Pierce Biotechnology. Bound proteins eluted with glutathione were analyzed by SDS-PAGE followed by Western blots probed with anti-N protein mouse monoclonal antibody J.3.3 (Hurst et al., 2010; Kuo et al., 2016); Western blot reagents were from Pierce Biotechnology.

Funding

This work was supported by National Institutes of Health (National Institute of Allergy and Infectious Diseases) grant R01 AI064603. The funding source had no role in the study design, collection and analysis of data, decision to publish, or preparation of the manuscript.

Declaration of competing interest

The authors declare no conflicts of interest.

CRediT authorship contribution statement

Cheri A. Koetzner: performed the experiments and analyzed the data, Writing – review &; editing. **Kelley R. Hurst-Hess:** performed the experiments and analyzed the data, Writing – review &; editing. **Lili Kuo:** performed the experiments and analyzed the data, Writing – review &; editing, edited the final, Writing – original draft. **Paul S. Masters:** conceived and designed the experiments and acquired, Funding acquisition, performed the experiments and analyzed the data, Writing – original draft, Writing – review &; editing, edited the final draft of the paper.

Acknowledgments

We thank the Wadsworth Center Applied Genomics Technology Core for DNA sequencing, the Media and Tissue Culture Core Facility for media preparation, and we are grateful to Pascal Lapierre of the Bioinformatics Core for genomic sequence analysis. We thank Ralph Baric (University of North Carolina) for providing the MHV full-length cDNA reverse genetics system.

References

Almazán, F., Galán, C., Enjuanes, L., 2004. The nucleoprotein is required for efficient coronavirus genome replication. J. Virol. 78, 12683–12688. https://doi.org/10.1128/JVI.78.22.12683-12688.2004.

Bah, A., Vernon, R.M., Siddiqui, Z., Krzeminski, M., Muhandiram, R., Zhao, C., Sonenberg, N., Kay, L.E., Forman-Kay, J.D., 2015. Folding of an intrinsically disordered protein by phosphorylation as a regulatory switch. Nature 519, 106–109. https://doi.org/10.1038/nature13999.

Bouhaddou, M., Memon, D., Meyer, B., et al., 2020. The global phosphorylation landscape of SARS-CoV-2 infection. Cell 182, 685–712. https://doi.org/10.1016/j.cell.2020.06.034 e19.

Casais, R., Thiel, V., Siddell, S.G., Cavanagh, D., Britton, P., 2001. Reverse genetics system for the avian coronavirus infectious bronchitis virus. J. Virol. 75, 12359–12369. https://doi.org/10.1128/JVI.75.24.12359-12369.2001.

Chang, C.K., Hou, M.H., Chang, C.F., Hsiao, C.D., Huang, T.H., 2014. The SARS coronavirus nucleocapsid protein - forms and functions. Antivir. Res. 103, 39–50. https://doi.org/10.1016/j.antiviral.2013.12.009.

Chang, C.K., Hsu, Y.L., Chang, Y.H., Chao, F.A., Wu, M.C., Huang, Y.S., Hu, C.K., Huang, T.H., 2009. Multiple nucleic acid binding sites and intrinsic disorder of severe acute respiratory syndrome coronavirus nucleocapsid protein: implications for ribonucleocapsid protein packaging. J. Virol. 83, 2255–2264. https://doi.org/10.1128/JVI.02001-08.

Chen, Y., Savinov, S.N., Mielech, A.M., Cao, T., Baker, S.C., Mesecar, A.D., 2015. X-ray structural and functional studies of the three tandemly linked domains of non-structural protein 3 (nsp3) from murine hepatitis virus reveal conserved functions. J. Biol. Chem. 290, 25293–25306. https://doi.org/10.1074/jbc.M115.662130.

Coley, S.E., Lavi, E., Sawicki, S.G., Fu, L., Schelle, B., Karl, N., Siddell, S.G., Thiel, V., 2005. Recombinant mouse hepatitis virus strain A59 from cloned, full-length cDNA replicates to high titers in vitro and is fully pathogenic in vivo. J. Virol. 79, 3097–3106. https://doi.org/10.1128/JVI.79.5.3097-3106.2005.

Cong, Y., Ulasli, M., Schepers, H., Mauthe, M., V'kovski, P., Kriegenburg, F., Thiel, V., de Haan, C.A.M., Reggiori, F., 2020. Nucleocapsid protein recruitment to replication-transcription complexes plays a crucial role in coronaviral life cycle. J. Virol. 94 https://doi.org/10.1128/JVI.01925-19 e01925-19.

Davidson, A.D., Williamson, M.K., Lewis, S., Shoemark, D., Carroll, M.W., Heesom, K.J., Zambon, M., Ellis, J., Lewis, P.A., Hiscox, J.A., Matthews, D.A., 2020. Characterisation of the transcriptome and proteome of SARS-CoV-2 reveals a cell passage induced in-frame deletion of the furin-like cleavage site from the spike glycoprotein. Genome Med. 12, 68. https://doi.org/10.1186/s13073-020-00763-0.

de Haan, C.A., Masters, P.S., Shen, X., Weiss, S., Rottier, P.J., 2002. The group-specific murine coronavirus genes are not essential, but their deletion, by reverse genetics, is attenuating in the natural host. Virology 296, 177–189. https://doi.org/10.1006/viro.2002.1412.

de Haan, C.A., Rottier, P.J., 2005. Molecular interactions in the assembly of coronaviruses. Adv. Virus Res. 64, 165–230. https://doi.org/10.1016/S0065-3527(05)64006-7.

Goebel, S.J., Taylor, J., Masters, P.S., 2004. The 3' cis-acting genomic replication element of the severe acute respiratory syndrome coronavirus can function in the murine coronavirus genome. J. Virol. 78, 7846–7851. https://doi.org/10.1128/JVI.78.14.7846-7851.2004.

Grossoehme, N.E., Li, L., Keane, S.C., Liu, P., Dann 3rd, C.E., Leibowitz, J.L., Giedroc, D. P., 2009. Coronavirus N protein N-terminal domain (NTD) specifically binds the transcriptional regulatory sequence (TRS) and melts TRS-cTRS RNA duplexes. J. Mol. Biol. 394, 544–557. https://doi.org/10.1016/j.jmb.2009.09.040.

Gui, M., Liu, X., Guo, D., Zhang, Z., Yin, C.C., Chen, Y., Xiang, Y., 2017. Electron microscopy studies of the coronavirus ribonucleoprotein complex. Protein Cell 8, 219–224. https://doi.org/10.1007/s13238-016-0352-8.

Hogue, B.G., Machamer, C.E., 2008. Coronavirus structural proteins and virus assembly. In: Perlman, S., Gallagher, T., Snijder, E.J. (Eds.), Nidoviruses. ASM Press, Washington, DC, pp. 179–200.

Hurst, K.R., Koetzner, C.A., Masters, P.S., 2009. Identification of in vivo-interacting domains of the murine coronavirus nucleocapsid protein. J. Virol. 83, 7221–7234. https://doi.org/10.1128/JVI.00440-09.

Hurst, K.R., Koetzner, C.A., Masters, P.S., 2013. Characterization of a critical interaction between the coronavirus nucleocapsid protein and nonstructural protein 3 of the viral replicase-transcriptase complex. J. Virol. 87, 9159–9172. https://doi.org/10.1128/JVI.01275-13.

Hurst, K.R., Kuo, L., Koetzner, C.A., Ye, R., Hsue, B., Masters, P.S., 2005. A major determinant for membrane protein interaction localizes to the carboxy-terminal domain of the mouse coronavirus nucleocapsid protein. J. Virol. 79, 13285–13297. https://doi.org/10.1128/JVI.79.21.13285-13297.2005.

Hurst, K.R., Ye, R., Goebel, S.J., Jayaraman, P., Masters, P.S., 2010. An interaction between the nucleocapsid protein and a component of the replicase-transcriptase complex is crucial for the infectivity of coronavirus genomic RNA. J. Virol. 84, 10276–10288. https://doi.org/10.1128/JVI.01287-10.

Keane, S.C., Giedroc, D.P., 2013. Solution structure of mouse hepatitis virus (MHV) nsp3a and determinants of the interaction with MHV nucleocapsid (N) protein. J. Virol. 87, 3502–3515. https://doi.org/10.1128/JVI.03112-12.

Keane, S.C., Liu, P., Leibowitz, J.L., Giedroc, D.P., 2012. Functional transcriptional regulatory sequence (TRS) RNA binding and helix destabilizing determinants of murine hepatitis virus (MHV) nucleocapsid (N) protein. J. Biol. Chem. 287, 7063–7073. https://doi.org/10.1074/jbc.M111.287763.

Klein, S., Cortese, M., Winter, S.L., Wachsmuth-Melm, M., Neufeldt, C.J., Cerikan, B., Stanifer, M.L., Boulant, S., Bartenschlager, R., Chlanda, P., 2020. SARS-CoV-2 structure and replication characterized by in situ cryo-electron tomography. Nat. Commun. 11, 5885. https://doi.org/10.1038/s41467-020-19619-7.

Knoops, K., Kikkert, M., Worm, S.H., Zevenhoven-Dobbe, J.C., van der Meer, Y., Koster, A.J., Mommaas, A.M., Snijder, E.J., 2008. SARS-coronavirus replication is supported by a reticulovesicular network of modified endoplasmic reticulum. PLoS Biol. 6, e226. https://doi.org/10.1371/journal.pbio.0060226.

Kuo, L., Hurst-Hess, K.R., Koetzner, C.A., Masters, P.S., 2016. Analyses of coronavirus assembly interactions with interspecies membrane and nucleocapsid protein chimeras. J. Virol. 90, 4357–4368. https://doi.org/10.1128/JVI.03212-15.

Kuo, L., Koetzner, C.A., Hurst, K.R., Masters, P.S., 2014. Recognition of the murine coronavirus genomic RNA packaging signal depends on the second RNA-binding domain of the nucleocapsid protein. J. Virol. 88, 4451–4465. https://doi.org/10.1128/JVI.03866-13.

Maier, H.J., Hawes, P.C., Cottam, E.M., Mantell, J., Verkade, P., Monaghan, P., Wileman, T., Britton, P., 2013. Infectious bronchitis virus generates spherules from zippered endoplasmic reticulum membranes. mBio 4, e00801–e00813. https://doi.org/10.1128/mBio.00801-13.

Masters, P.S., Koetzner, C.A., Kerr, C.A., Heo, Y., 1994. Optimization of targeted RNA recombination and mapping of a novel nucleocapsid gene mutation in the coronavirus mouse hepatitis virus. J. Virol. 68, 328–337. https://doi.org/10.1128/JVI.68.1.328-337.1994.

Mihelc, E.M., Baker, S.C., Lanman, J.K., 2021. Coronavirus infection induces progressive restructuring of the endoplasmic reticulum involving the formation and degradation of double membrane vesicles. Virology 556, 9–22. https://doi.org/10.1016/j.virol.2020.12.007.

Neuman, B.W., 2016. Bioinformatics and functional analyses of coronavirus nonstructural proteins involved in the formation of replicative organelles. Antivir. Res. 135, 97–107. https://doi.org/10.1016/j.antiviral.2016.10.005.

Neuman, B.W., Joseph, J.S., Saikatendu, K.S., Serrano, P., Chatterjee, A., Johnson, M.A., Liao, L., Klaus, J.P., Yates 3rd, J.R., Wüthrich, K., Stevens, R.C., Buchmeier, M.J., Kuhn, P., 2008. Proteomics analysis unravels the functional repertoire of coronavirus nonstructural protein 3. J. Virol. 82, 5279–5294. https://doi.org/10.1128/JVI.02631-07.

Peng, T.Y., Lee, K.R., Tarn, W.Y., 2008. Phosphorylation of the arginine/serine dipeptide-rich motif of the severe acute respiratory syndrome coronavirus nucleocapsid protein modulates its multimerization, translation inhibitory activity and cellular localization. FEBS J. 275, 4152–4163. https://doi.org/10.1111/j.1742-4658.2008.06564.x.

Schelle, B., Karl, N., Ludewig, B., Siddell, S.G., Thiel, V., 2005. Selective replication of coronavirus genomes that express nucleocapsid protein. J. Virol. 79, 6620–6630. https://doi.org/10.1128/JVI.79.11.6620-6630.2005.

Serrano, P., Johnson, M.A., Almeida, M.S., Horst, R., Herrmann, T., Joseph, J.S., Neuman, B.W., Subramanian, V., Saikatendu, K.S., Buchmeier, M.J., Stevens, R.C., Kuhn, P., Wüthrich, K., 2007. Nuclear magnetic resonance structure of the N-terminal domain of nonstructural protein 3 from the severe acute respiratory syndrome coronavirus. J. Virol. 81, 12049–12060. https://doi.org/10.1128/JVI.00969-07.

Sims, A.C., Ostermann, J., Denison, M.R., 2000. Mouse hepatitis virus replicase proteins associate with two distinct populations of intracellular membranes. J. Virol. 74, 5647–5654. https://doi.org/10.1128/jvi.74.12.5647-5654.2000.

Snijder, E.J., Limpens, R.W.A.L., de Wilde, A.H., de Jong, A.W.M., Zevenhoven-Dobbe, J. C., Maier, H.J., Faas, F.F.G.A., Koster, A.J., Bárcena, M., 2020. A unifying structural and functional model of the coronavirus replication organelle: tracking down RNA synthesis. PLoS Biol. 18, e3000715 https://doi.org/10.1371/journal.pbio.3000715.

Sola, I., Almazán, F., Zúñiga, S., Enjuanes, L., 2015. Continuous and discontinuous RNA synthesis in coronaviruses. Annu Rev Virol 2, 265–288. https://doi.org/10.1146/annurev-virology-100114-055218.

Stertz, S., Reichelt, M., Spiegel, M., Kuri, T., Martínez-Sobrido, L., García-Sastre, A., Weber, F., Kochs, G., 2007. The intracellular sites of early replication and budding of SARS-coronavirus. Virology 36, 304–315. https://doi.org/10.1016/j.virol.2006.11.027.

Tannous, B.A., Kim, D.E., Fernandez, J.L., Weissleder, R., Breakefield, X.O., 2005. Codon-optimized Gaussia luciferase cDNA for mammalian gene expression in culture and in vivo. Mol. Ther. 11, 435–443. https://doi.org/10.1016/j.ymthe.2004.10.016.

Thiel, V., Herold, J., Schelle, B., Siddell, S.G., 2001. Viral replicase gene products suffice for coronavirus discontinuous transcription. J. Virol. 75, 6676–6681. https://doi.org/10.1128/JVI.75.14.6676-6681.2001.

Ulasli, M., Verheije, M.H., de Haan, C.A., Reggiori, F., 2010. Qualitative and quantitative ultrastructural analysis of the membrane rearrangements induced by coronavirus. Cell Microbiol. 12, 844–861. https://doi.org/10.1111/j.1462-5822.2010.01437.x.

van der Meer, Y., Snijder, E.J., Dobbe, J.C., Schleich, S., Denison, M.R., Spaan, W.J., Locker, J.K., 1999. Localization of mouse hepatitis virus nonstructural proteins and RNA synthesis indicates a role for late endosomes in viral replication. J. Virol. 73, 7641–7657. https://doi.org/10.1128/JVI.73.9.7641-7657.1999.

Verma, S., Bednar, V., Blount, A., Hogue, B.G., 2006. Identification of functionally important negatively charged residues in the carboxy end of mouse hepatitis coronavirus A59 nucleocapsid protein. J. Virol. 80, 4344–4355. https://doi.org/10.1128/JVI.80.9.4344-4355.2006.

Wolff, G., Limpens, R.W.A.L., Zevenhoven-Dobbe, J.C., Laugks, U., Zheng, S., de Jong, A. W.M., Koning, R.I., Agard, D.A., Grünewald, K., Koster, A.J., Snijder, E.J., Bárcena, M., 2020. A molecular pore spans the double membrane of the coronavirus replication organelle. Science 369, 1395–1398. https://doi.org/10.1126/science.abd3629.

Wu, C.H., Yeh, S.H., Tsay, Y.G., Shieh, Y.H., Kao, C.L., Chen, Y.S., Wang, S.H., Kuo, T.J., Chen, D.S., Chen, P.J., 2009. Glycogen synthase kinase-3 regulates the phosphorylation of severe acute respiratory syndrome coronavirus nucleocapsid protein and viral replication. J. Biol. Chem. 284, 5229–5239. https://doi.org/10.1074/jbc.M805747200.

Yao, H., Song, Y., Chen, Y., Wu, N., Xu, J., Sun, C., Zhang, J., Weng, T., Zhang, Z., Wu, Z., Cheng, L., Shi, D., Lu, X., Lei, J., Crispin, M., Shi, Y., Li, L., Li, S., 2020. Molecular architecture of the SARS-CoV-2 virus. Cell 183, 730–738. https://doi.org/10.1016/j.cell.2020.09.018 e13.

Ye, Q., West, A.M.V., Silletti, S., Corbett, K.D., 2020. Architecture and self-assembly of the SARS-CoV-2 nucleocapsid protein. Protein Sci. 29, 1890–1901. https://doi.org/10.1002/pro.3909.

Yount, B., Curtis, K.M., Baric, R.S., 2000. Strategy for systematic assembly of large RNA and DNA genomes: transmissible gastroenteritis virus model. J. Virol. 74, 10600–10611. https://doi.org/10.1128/jvi.74.22.10600-10611.2000.

Yount, B., Curtis, K.M., Fritz, E.A., Hensley, L.E., Jahrling, P.B., Prentice, E., Denison, M. R., Geisbert, T.W., Baric, R.S., 2003. Reverse genetics with a full-length infectious cDNA of severe acute respiratory syndrome coronavirus. Proc. Natl. Acad. Sci. U.S.A. 100, 12995–13000. https://doi.org/10.1073/pnas.1735582100.

Yount, B., Denison, M.R., Weiss, S.R., Baric, R.S., 2002. Systematic assembly of a full-length infectious cDNA of mouse hepatitis virus strain A59. J. Virol. 76, 11065–11078. https://doi.org/10.1128/jvi.76.21.11065-11078.2002.

Zúñiga, S., Cruz, J.L., Sola, I., Mateos-Gómez, P.A., Palacio, L., Enjuanes, L., 2010. Coronavirus nucleocapsid protein facilitates template switching and is required for efficient transcription. J. Virol. 84, 2169–2175. https://doi.org/10.1128/JVI.02011-09.